JOURNAL OF APPLIED ELECTROCHEMISTRY 18 (1988) 768–780

Laminar radial flow electrochemical reactors. I. Flow fields

F. B. THOMAS

Hycal Energy Research Labs Ltd, 1338 A, 36th Avenue, N.E. Calgary, Alberta, Canada T2E 6T6

P. A. RAMACHANDRAN, M. P. DUDUKOVIC

Chemical Reaction Engineering Laboratory, Department of Chemical Engineering, Washington University, St Louis, MO 63130, USA

R. E. W. JANSSON

Monsanto Corporation, 800 North Lindbergh Blvd, St Louis, MO 63167, USA

Received 4 January 1988; revised 1 April 1988

The velocity fields of three laminar radial flow electrochemical reactors are modeled using numerical and semi-analytical techniques. The capillary gap cell configuration is modeled using Galerkin finite element (GFEM) analysis and the asymptotic form of its velocities presented. An approximate asymptotic expression for entry length is also derived and compared to predicted entry lengths from the GFEM. Qualitative agreement is achieved. Two areas of flow separation are observed, their location being a function of gap width, flow Reynolds number (*Re*) and inlet pipe diameter. The rotating electrolyzer (REL) flow field is also simulated with the GFEM model. The insensitivity of the REL radial velocity profiles as a function of flow rate is shown. The shape of the radial velocity profiles and the degree of separation of the radial velocity jets are shown to be determined by the Taylor number (being the ratio of half-gap width over the theoretical boundary layer thickness). The asymptotic entry length solution is shown to provide a better estimate for this cell than for the capillary gap cell. Unlike the previous cells the pump cell shows less asymptotic behavior and is therefore more difficult to simulate. The GFEM approach is usually too costly for this cell and therefore perturbation techniques are applied. The resulting semi-analytical solution adequately represents laminar pump cell velocity profiles over a broad range of parameter values and is very short and easy to implement. One high Taylor number simulation is performed using the GFEM and the previously reported decoupling of electrodic mass transfer is interpreted via velocity profiles.

Nomenclature

a	gap width
Q	volumetric flow rate ($m^3\,s^{-1}$)
r	dimensionless radius
R	radius (m)
Re	Reynolds number ($v_c a/\nu$)
Re_{gap}	gap Reynolds number ($a^2\omega/\nu$)
Re_θ	rotational Reynolds number ($\omega R_0^2/\nu$)
Sc	Schmidt number (ν/D)
spin	dimensionless group (Equation 8)
t	time (s)
v_c	characteristic velocity ($m\,s^{-1}$) two defined: for FEM analysis it was $Q/\pi b^2$ for Perturbation analysis $6Q/(2\pi R_{in} a)$
v_r	dimensionless radial velocity
v_z	dimensionless axial velocity
v_θ	dimensionless azimuthal velocity
V	velocity ($m\,s^{-1}$)
z	dimensionless axial distance

Greek symbols

α	Taylor number (Equation 7)
ε	ratio of characteristic lengths (a/R_0)
μ	viscosity ($kg\,m^{-1}\,s$)
π	constant
ϱ	density ($kg\,m^{-3}$)
θ	azimuthal direction
ν	kinematic viscosity ($m^2\,s^{-1}$)
ω	angular velocity ($rad\,s^{-1}$)

1. Introduction

As a result of the ongoing search for improved electrochemical reactors, many alternative designs have surfaced. Of these, the radial flow parallel disc designs show many advantages over the more conventional parallel plate configurations. Figure 1 describes the general geometry of these electrochemical reactors. The general improvement possessed by the radial flow design is that the gap width can be adjusted. Since gap

0021-891X/88 $03.00 + .12

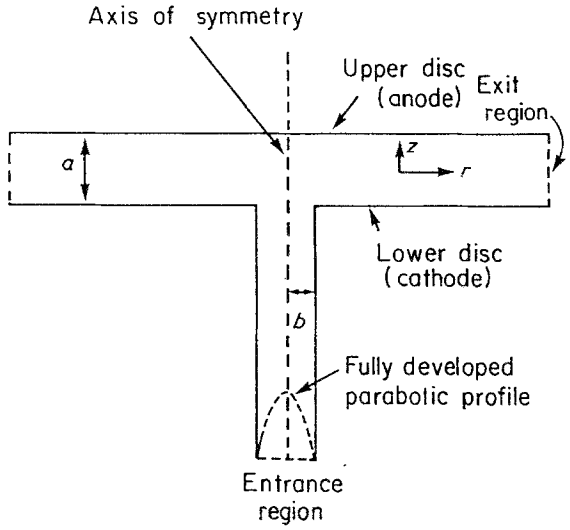

Fig. 1. Radial flow cell geometry.

width alters the ratio between electrode surface area and electrolyte volume, one can exercise greater control over the contribution of electrodic reaction to the overall process. In addition, the interelectrode voltage drop (solution *IR* loss), being proportional to the gap width, can also be readily adjusted. These factors, with their corresponding impact on the figures of merit, suggest that radial flow cells may become more popular as preferred reactor types in future electrochemical applications.

The flow rates used in many electrochemical applications are large enough that the flows are adequately described as convection dominated. In such instances, the transport of species present in the flow has negligible influence on the velocity profiles. Therefore, most of the relevant work in defining the radial cell hydrodynamics originates in areas other than electrochemical engineering, where only fluid flow was considered regardless of possible application. This paper is therefore an attempt at summarizing the radial flow cell flow fields and presenting them in an accurate and unified manner.

There are three main reactors of this configuration. The first, and most common, is the capillary gap cell (CGC), where both discs are stationary; electrolyte flows radially outwards between the two parallel discs. The second type is the rotating electrolyzer (REL) which is similar to the CGC except that it also includes coaxial disc rotation. The third type is the pump cell (PC) which has one disc spinning and one disc stationary. The rotational set-up determines the hydrodynamic behavior which in turn influences reactor performance. Jansson and co-workers [1–5] have shown the differences in cell performance for numerous applications. A brief summary of previous flow field studies will now be given.

2. Previous work

2.1. *Capillary gap cell*

For this case both discs are stationary and, after a certain entry length, parabolic flow results (in the laminar regime). Mochizuki *et al.* [6] observed oscillatory behavior at low flow Reynolds numbers ($Re = 16$ according to the definition in this work). These were observed in the presence of slight heat transfer effects. Szeri *et al.* [7] performed experimental and theoretical work on the stationary case as part of a detailed investigation into flow between parallel discs. Operating the stationary case over a two-fold range in flow rate (64.55 and 135.7 $cm^3 s^{-1}$) at a gap width of 3.175 mm, they failed to observe any flow separation. Indeed, they indicate 'we were unable to show experimentally flow separation at the walls under any conditions'. The full range of operating conditions was not provided, but even so this result is curious. The simplified theory of Moller [8] predicts conditions of disc spacing and flow which would produce adverse pressure gradients and incite flow separation. Ashworth and Jansson [4] indicate that for a gap to disc radius ratio of 8.7×10^{-4} and a Reynold's number of 5.03×10^5 the radial gradient is always favorable (negative). However for a gap four times larger (1 mm compared with 0.25 mm) an unfavorable gradient was observed over almost all of the disc surfaces. Coupling this adverse pressure profile with the radial deceleration, separation would be expected. Indeed Yang [9] has reported time dependent upper and lower regions of separation forming at the disc surfaces at different radii. This tends to support the expectation of flow separation and make the lack of such, in the work of Szeri *et al.*, appear even more anomalous. Since the full range of parameters employed in that work is not stated, it is difficult to say any more. The only mitigating factor is that the results of Ref. [4] were in the turbulent regime (although the pressure profiles were somewhat the same for turbulent and laminar flows) and the observations of Yang [9] were made with slight natural convection influences. The work of Szeri *et al.* was over some range of parameters but the range of actual values was not included in that paper.

2.2. *Pump cell*

Early work was done by Bayley and Owens [10] on disc flows where one disc was spinning and one stationary, but their work was for turbulent flows where flow Reynolds numbers were much higher than rotational Reynolds numbers, and hence the behavior differed little from that of a turbulent capillary gap cell. Other work done earlier has been restricted to rotation of a single disc in a semi-infinite fluid; an example of this is the work of von Karman described by Schlichting [11]. Therein, von Karman 'assumed' forms for the velocities: v_r assumed to be $r\omega f(z)$, v_θ as $r\omega g(z)$ and v_z as $(\nu\omega)^{0.5} h(z)$. A set of non-linear, simultaneous, ordinary differential equations result, which provide a very adequate representation for the physical system studied (rotating disc in a semi-infinite medium). Due to the presence of the stationary disc in the pump cell, this same analysis is not applicable,

although some similarities are present, as will be illustrated later in this paper.

Much work was done applying these von Karman transformations to two closely spaced infinite and finite discs [12–14]. Multiple solutions were found depending primarily upon a gap Reynolds number (see Ref. [14]). The stability of these solutions is not commented on however.

Adams and Szeri [15] developed a numerical solution scheme based on the Galerkin–Kantorovich method in the axial direction and orthogonal collocation in the radial direction. Szeri *et al.* [7] then expanded on Adams *et al.*'s [15] previous work, including experimental results. They studied the cases of zero rotation, one disc spinning, co-rotational coaxial discs as well as counter-rotating coaxial discs. The experimental procedure and apparatus used is well documented in that reference. The theoretical model developed was based on Galerkin time integration, using B-splines for the spatial terms. On the basis of both experimental and theoretical investigation, they conclude that the flows observed are unique and reproducible irrespective of the starting conditions, and therefore the other members of the family of multiple solutions described by Holodniok *et al.* [14] are unstable under all conditions. The only limiting flow observed approached the Batchelor-type scenario [12], and the Stewartson branch [13] was never confirmed in their work.

2.3. *Rotating electrolyzer*

Kreith [16], in studying heat transfer between parallel discs developed a series solution to the problem of coaxial co-rotating discs. He suggested that for a given flow rate, as rotational speed is increased, radial velocity jets appear close to the disc surfaces. In addition, at a Taylor number (defined as $0.5a(\omega/\nu)^{0.5}$ – representing the ratio of half-gap width divided by the characteristic boundary layer thickness) above π there would be a zone of zero velocity beginning at the mid-plane between the discs. Later, Jansson [3] extended the series form of Kreith to include third-order terms. Experimental work was also reported [3, 17] and the agreement between theory and experiment was quite good. The advantage of the third-order approximation of Jansson [3] was especially obvious at large Taylor numbers (larger than about 7) when compared to Kreith's first-order system. Simek and Roušar [18] extended the same analysis to include fifth-order terms, the only improvement being apparent at small radii only. However, some numerical problems were encountered contributing to reverse flows in the regions close to the discs. The authors conclude that this is a numerical artifice inconsistent with reality.

The arguments of Holodniok *et al.* [14] are also relevant to this configuration. However, in the light of the findings of Szeri *et al.* [7], it is thought that the multiple solution scenario would not be the case in reality, all but one solution probably being unstable and never appearing.

In the light of these findings, it was apparent that a simplified representation of the three radial cell velocity profiles would be difficult to achieve, if not impossible, and therefore to adequately describe convection effects in the electrochemical reactors of interest, recourse would have to be made to numerical analysis. The next section descibes the formulation used, including the equations, defined dimensionless groups and boundary conditions applied, and numerical technique employed.

3. Model formulation

Incompressible flows are described by the Navier–Stokes equations. The derivation of these equations is detailed elsewhere (for example Schlichting [11]) and is therefore not discussed here. Defining the following dimensionless quantities as

$$v_r = \frac{v_r^*}{v_c}; \quad v_z = \frac{v_z^*}{v_c}; \quad v_\theta = \frac{v_\theta^*}{R_0\omega};$$

$$P = \frac{P^* - rg_zZ}{rv_c^2}; \quad r = \frac{R}{R_0}; \quad z = \frac{Z}{a};$$

$$\varepsilon = \frac{a}{R_0}; \quad Re = \frac{v_c a}{\nu}; \quad \text{spin} = \left(\frac{R_0\omega}{v_c}\right)^2$$

where v_c is defined as $Q/(\pi b^2)$ and b is the radius of the inlet pipe. Substituting into the Navier–Stokes equations ones obtains

$$v_r\frac{\partial v_r}{\partial r} - \text{spin}\,\frac{v_\theta^2}{r} + \frac{v_z\partial v_r}{\varepsilon\partial z} = -\frac{\partial P}{\partial r} + \frac{1}{Re}\left(\varepsilon\left(\frac{\partial^2 v_r}{\partial r^2} + \frac{\partial v_r}{r\partial r} - \frac{v_r}{r^2}\right) + \frac{\partial^2 v_r}{\varepsilon\partial z^2}\right) \tag{1}$$

$$v_r\frac{\partial v_\theta}{\partial r} + \frac{v_r v_\theta}{r} + \frac{v_z}{\varepsilon}\frac{\partial v_\theta}{\partial z} = \frac{1}{Re}\left(\varepsilon\left(\frac{\partial^2 v_\theta}{\partial r^2} + \frac{\partial v_\theta}{r\partial r} - \frac{v_\theta}{r^2}\right) + \frac{\partial^2 v_\theta}{\varepsilon\partial z^2}\right) \tag{2}$$

$$v_r\frac{\partial v_z}{\partial r} + \frac{v_z}{\varepsilon}\frac{\partial v_z}{\partial z} = -\frac{\partial P}{\partial z} + \frac{1}{Re}\left(\varepsilon\left(\frac{\partial^2 v_z}{\partial r^2} + \frac{\partial v_z}{r\partial r}\right) + \frac{1}{\varepsilon}\frac{\partial^2 v_z}{\partial z^2}\right) \tag{3}$$

$$\frac{\partial(rv_r)}{\partial r} + \frac{1\partial(rv_z)}{\varepsilon\partial z} = 0 \tag{4}$$

The dimensionless group 'spin' can also be expressed as a product of the three, more conventional, dimensionless groups, rotational Reynolds number Re_θ, flow Reynolds number (Re) and Taylor number (α). These are defined as

$$Re_\theta = \frac{R_0^2\omega}{\nu} \tag{5}$$

$$Re = \frac{v_c a}{\nu} \tag{6}$$

$$\alpha = \left(\frac{a^2\omega}{4\nu}\right)^{0.50} \tag{7}$$

$$\text{spin} = \frac{4Re_\theta\alpha^2}{Re^2} = 4\left(\frac{R_0^2\omega}{\nu}\right)\left(\frac{a^2\omega}{4\nu}\right)\left(\frac{\nu^2}{v_c^2a^2}\right) \tag{8}$$

Therefore on the basis of Re, Re_θ, α, ε and one other parameter, the radius of the inlet pipe, the problem is defined. To complete the formulation, the boundary conditions must be specified.

At the inlet pipe entrance, some distance below the bottom disc, fully developed laminar pipe flow is specified. That is, v_z assumes a parabolic profile as a function of pipe radius $(2 \times v_c(1 - (R/b)^2)$ where v_c is as defined previously: $v_c = Q/\pi b^2$. At this point $v_r = v_\theta = 0$ also.

The axis of symmetry provides the following boundary conditions:

$$\begin{aligned} v_r &= 0 \\ \frac{\partial v_\theta}{\partial r} &= 0 \\ \frac{\partial v_z}{\partial r} &= 0 \end{aligned} \tag{9}$$

The solid surfaces are no-slip boundaries and therefore

$$\begin{aligned} v_r &= 0 \\ v_z &= 0 \\ v_\theta &= r \end{aligned} \tag{10}$$

The only boundary which is somewhat subject to controversy is the exit end. Usually in electrochemical cells, the effluent from the reactor empties into a larger tank containing the same fluid. To rigorously define the boundary the whole system would have to be simulated. For the purpose of this work, a simplified approach will be taken since the exit boundary conditions are not of extreme importance, due to the coefficient of the second-order radii terms (as will be demonstrated in the next section), and from experience gained from running the model, which will also be commented on when the model results are reported.

3.1. *Capillary gap cell*

In this cell, the axial velocity approaches a small value beyond the entry region. From continuity, since $v_z \approx 0$, $\partial v_z/\partial z = 0$, then

$$\frac{\partial v_r}{\partial r} = -\left.\frac{v_r}{r}\right|_{R_0} \tag{11}$$

at the exit. Hence in the iterative scheme, as the correct value of v_r is approached, the true boundary condition will be approximated.

The v_z boundary condition is $\partial v_z/\partial r = 0$ and since there is no rotation in the capillary gap cell v_θ is always zero.

3.2. *Pump cell*

The form of the exit boundary conditions for this cell was less clear, since v_z was finite and could not be assumed to be zero. Therefore $\partial v_z/\partial z$ was not zero and boundary information could not be gained by the method used in the CG cell. From some semi-analytical work, to be described later in this paper, a few trends became apparent, although they were strictly only approximate. If the radial velocity were a function of $r \times f(\omega, z)$ then $\partial v_r/\partial r$ could be approximated by

$$\frac{\partial v_r}{\partial r} = \left.\frac{v_r}{r}\right|_{R_0} \tag{12}$$

since v_r at R_0 would be $R_0 \times f(\omega, z)$ and as convergence was obtained, v_r/r at $r = R_0$ would approach the function $f(\omega, z)$. Hence, in an iterative manner the v_r boundary condition could be approached. The same was then applied to the v_θ boundary condition with the same reasoning. Therefore for v_θ

$$\frac{\partial v_\theta}{\partial r} = \left.\frac{v_\theta}{r}\right|_{R_0} \tag{13}$$

For the v_z condition it became apparent that $\partial v_z/\partial r = 0$ would be adequate.

3.3. *Rotating electrolyzer*

Here the axial velocities became small (three orders of magnitude smaller than the other velocities) and hence the same v_r condition was invoked – Equation 11.

The azimuthal component of velocity was determined using the boundary condition 13 (although using $\partial v_\theta/\partial r = 1$ provided similar results). The v_z boundary condition was the same as for the CG cell, *viz.* $\partial v_z/\partial r = 0$.

The pressure did not have to be specified anywhere, since it had been included in the integration by parts in developing the generalized finite element formulation. Gresho *et al.* [19] comment on this as the only consistent manner of treating the pressure term.

3.4. *Numerical formulation*

The equations, specification of the dimensionless groups and the establishment of the boundary conditions complete the model formulation. A Galerkin finite element (GFEM) program was then constructed to solve the above system of equations.

Since the equations are nonlinear the solution procedure must necessarily be iterative in nature. Initially, Picard iteration was used, but this was inefficient for Re values above 50 and would not converge for Taylor numbers above 3.0. The Newton–Raphson method was then incorporated to enhance convergence. In the GFEM formulation, the discrete values of the variables at the nodes are the unknowns and therefore partial differentiation (in establishing the Jacobian) is with respect to these [19, 20]. This provided much better convergence; the solution was usually commenced with three or four iterations of Picard iteration, followed by two or three Newton–Raphson steps. For higher nonlinearities, convergence

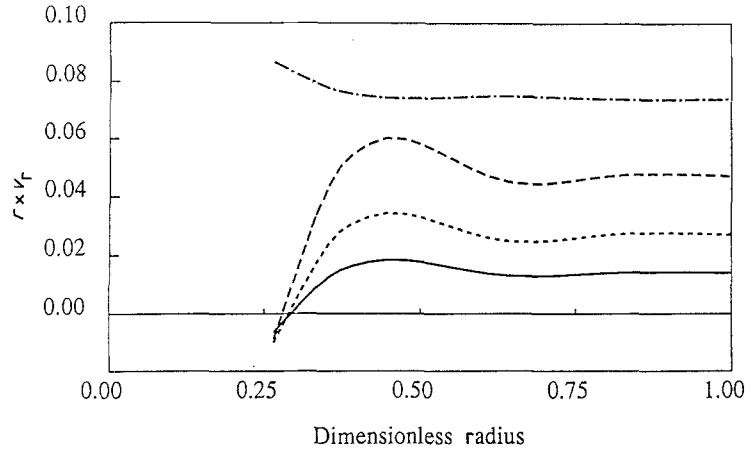

Fig. 2. Entry length information. Capillary gap cell: gap = 6.4 mm, and flow rate = 3.8×10^{-6} m^{3}s^{-1}. (——) z = 0.05, 0.95; (– – – –) z = 0.10, 0.90; (— – —) z = 0.20, 0.80; (—·—) z = 0.50.

was obtained by using less nonlinear converged solutions as restart initial conditions for the more nonlinear cases. The frontal solution subroutine of Hood [21] for asymmetric matrices was employed for the solution of the resulting large set of simultaneous equations.

4. Flow field results

The results of the model are reported and discussed according to the cell type.

4.1. *Capillary gap cell*

Computer runs were done for this case and the general forms of velocity profiles were confirmed. The flow is initially purely axial in the inlet pipe, with no radial component (for stationary discs no azimuthal velocity was present anywhere). After rounding the sharp corner, after a certain entry length, the fluid flows in fully developed radial outflow, it being parabolic with respect to the z coordinate. In addition, when the product rv_r is plotted for numerous z values, one sees that rv_r approaches a function of z only at large enough radius, and v_z approaches zero. Figure 2 presents the rv_r asymptotes for this cell and comparison of the values of the asymptotes shows that they obey a parabolic profile.

Once the entry region is accounted for the flow is very simple. Because of this, most of the experimental work done to date, along with subsequent theoretical analysis, has been performed assuming that the flow was fully developed. However, there is very little knowledge concerning the extent of the entry zone. To help in quantifying this, computer runs were done in which flow rate, gap width and inlet pipe radius were changed. The rv_r function was then plotted for these different conditions. The radius at which the product rv_r became a function of z only was then interpreted as the entry length. A number of runs were done as suggested, altering the inlet radius from 1.2 to 9 mm, the gap width from 0.60 to 6.3 mm and the flow rate from 6.8×10^{-8} to 1.25×10^{-5} m^{3}s^{-1}. An approximate asymptotic solution was also derived and then used to calculate required entry lengths. The form of the asymptotic entry length solution was

$$R_{\text{entry}} = \left[\frac{Qa}{5\pi\nu}\right]^{1/2} \tag{14}$$

Table 1 presents a comparison of some entry length values for different parameter ranges.

Although the results are of the same order of magnitude, the comparison is poor. The asymptotic entry length solution shows that the entry region is a function of flow rate, gap width and the fluid kinematic viscosity. The FEM calculations also indicate, however, that the entry lenth is a function of inlet radius; decreasing with increasing inlet radius. A few forms of correlation were tried but no attempted combination provided a reasonable collapse of the GFEM-computed entry lengths. The comparison is improved by adding R_{in} to the asymptotic results, this being intuitively consistent in light of the geometry.

With the given cell geometry (the fluid flows up the pipe and then out radially between the two parallel discs), and since the corner is sharp, there is separation and an eddy formed at that point. At low flow Reynolds numbers the region of separation was small. However, at increasing Re the region of separation increased. For an Re of 100 the vortex ended at r = 0.44; for Re equal to 220 it extended to r = 0.59 and at Re equal to 420 it ended at 0.68 dimensionless radius (using an aspect ratio (R_0/a) of 10). As anticipated the vortices, at their highest point, influenced 30, 40 and 50% of the interelectrode gap at Reynolds numbers of 100, 200 and 420, respectively.

Table 1. Comparison of entry lengths

1. R_{in} = 2.4 mm, R_0 = 12 mm, gap = 0.60 mm, $Q = 6.8e^{-07}$ m^{3}s^{-1}	
	Asymptotic entry length = 5.1 mm
	FEM length = 8.7 mm
2. R_{in} = 1.2 mm, R_0 = 24 mm, gap = 1.2 mm, $Q = 2.0e^{-06}$ m^{3}s^{-1}	
	Asymptotic entry length = 12.3 mm
	FEM length = 21.1 mm
3. R_{in} = 5.0 mm, R_0 = 50 mm, gap = 1.0 mm, $Q = 12.5e^{-06}$ m^{3}s^{-1}	
	Asymptotic entry length = 28.2 mm
	FEM length = 42.0 mm

One important point is that at *Re* equal to 220 and 420 another eddy forms further downstream. However, it forms at the upper disc. In addition, it forms at approximately the point where the eddy from the bottom disc terminates. For example, at $Re = 220$, the bottom vortex stopped at $r = 0.59$ and the top one commenced at the same radius. At $Re = 420$ the bottom one ceased at $r = 0.69$ and the top one formed at $r = 0.66$. The duration of this upper eddy also increased with *Re*. At $Re = 220$, the upper one ended at 0.66 (short lived), while at $Re = 420$, it ceased at $r = 0.94$.

Beyond a Reynolds number of 420, convergence was very difficult to obtain; the velocity values appeared to vary around a certain magnitude but tended to cycle. In the light of what Mochizuki *et al.* [6] reported, this may be due to the time-dependent physics of the problem. Moreover, Yang [9] has indicated that eddy formation is a cyclic time-dependent phenomenon. He also reported the general upper and lower vortex regions, as were observed in the present finite element simulation (steady state), alternating in a regular manner.

These results of Yang would lend credence to the predictions of the present model and would also support the need for a transient analysis for intermediate to high Reynolds numbers.

4.2. *Pump cell*

The FEM program was then applied to the pump cell with conditions given in Fig. 6 of Szeri *et al.* [7]. This flow represents a finite through-flow with the characteristic areas of positive and negative radial velocities. Figure 3 presents a comparison of the experimental data of Szeri *et al.*, their numerical results and this work. This present model provides as close a comparison to experimental data as the numerical approach of Szeri. They indicated in a previous paper [15] that convergence was possible for a gap rotational Reynolds number of 140, whereas convergence was obtained up to 540 in this work. The Newton–Raphson FEM might therefore be superior to the approach which the previous authors employed, although no CPU time comparison is possible. The agreement, compared to previous work, is close, which lends credence to results generated herein.

As opposed to the capillary gap cell the radial velocity does not approach an asymptote and the axial velocities are finite and can be quite large (although at least an order of magnitude smaller than the radial and azimuthal components). This made modelling the PC flow field more difficult than the capillary gap cell, since once the flow was fully developed, an algebraic extrapolation procedure (based on rv_r becoming a function of z only) was not as readily apparent as in the capillary gap cell. Even with aspect ratios ($1/\varepsilon$) as large as 40, no asymptotic behavior was observed in the PC velocities that would allow a simplified extrapolation technique for velocity determination at larger radii. This would be a serious limitation since the

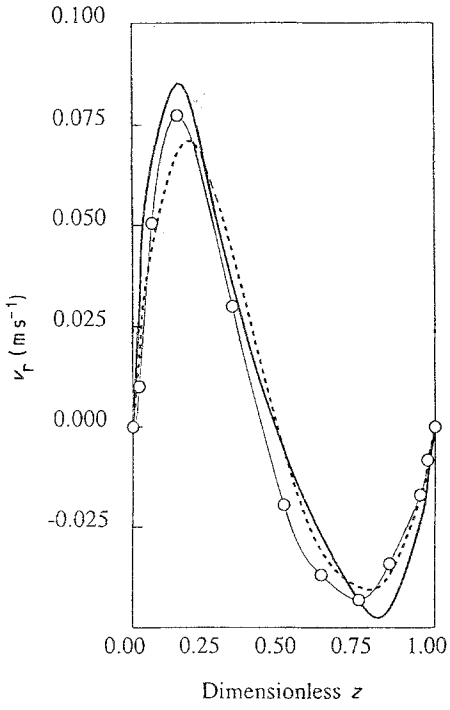

Fig. 3. Pump cell comparison at 44.4 r.p.m: ($\alpha = 3.42$) radial velocities at $R = 12.7$ cm, gap = 3.18 mm and flow rate = 2.0×10^{-5} m^3 s^{-1}. (——) FEM model; (– – – –) Szeri's model; (○) Experimental data.

FEM would have to be used throughout the flow field computation, and the storage and CPU time requirements would soon become excessive. Indeed, even at $\varepsilon = 0.025$, at a $Re_\theta = 10^4$, 321 elements were required to resolve the flow field in the PC (4600 equations), requiring approximately 230 CPU minutes on a Vax 11/780 computer. In industrial cells aspect ratios are often as large as 1000 ($\varepsilon = 0.001$) and hence computer costs would be prohibitive unless recourse to a super computer was available. Even then, the utility of such calculations might be questionable.

Due to the applied nature of this work, a semi-analytical scheme was then sought, hoping that a representative flow field solution might be possible, which could then be employed in the subsequent reactor computations to be described in later papers.

Using Equations 1–4 the order of magnitude of the second order r terms is ε^3 (since $1/Re \approx \varepsilon$) and since ε is at least as small as 0.10, these terms were dropped. It is thought that this is a good assumption since usually $\varepsilon \approx 0.01$ and therefore negligible error should be introduced by this omission. The equations then become

$$v_r \frac{\partial v_r}{\partial r} - \text{spin}\,\frac{v_\theta^2}{r} + \frac{v_z}{\varepsilon}\frac{\partial v_r}{\partial z} = -\frac{\partial P}{\partial r} + \frac{1}{\varepsilon Re}\frac{\partial^2 v_r}{\partial z^2} \tag{15}$$

$$v_r \frac{\partial v_\theta}{\partial r} + \frac{v_r v_\theta}{r} + \frac{v_z}{\varepsilon}\frac{\partial v_\theta}{\partial z} = \frac{1}{\varepsilon Re}\frac{\partial^2 v_\theta}{\partial z^2} \tag{16}$$

$$v_r \frac{\partial v_z}{\partial r} + \frac{v_z}{\varepsilon}\frac{\partial v_z}{\partial z} = -\frac{\partial P}{\partial z} + \frac{1}{\varepsilon Re}\frac{\partial^2 v_z}{\partial z^2} \tag{17}$$

$$\frac{v_r}{r} + \frac{\partial v_r}{\partial r} + \frac{1}{\varepsilon}\frac{\partial v_z}{\partial z} = 0 \tag{18}$$

Only one other assumption was made. It was noticed that in some previous numerical results, the pressure did not differ too significantly from hydrostatic pressure (in the axial direction). If this is assumed, then $\partial P/\partial z$ would be approximately zero due to the dimensionless pressure definition. Hence, the pressure term retained in the system, $\partial P/\partial r$ in Equation 16, becomes dP/dr, P being a function of radius only. A similarity solution was attempted using different stretching transformations. The azimuthal velocity boundary conditions would not collapse, however, and this approach had to be dismissed.

Perturbation was then employed using $\varepsilon = a/R_0$ as the perturbation parameter. Each of the dependent variables was expanded as a series. That is,

$$v_r = v_{r0} + \varepsilon v_{r1} + \varepsilon^2 v_{r2} + \ldots \quad (19)$$

$$v_\theta = v_{\theta 0} + \varepsilon v_1 + \varepsilon^2 v_{\theta 2} + \ldots \quad (20)$$

$$v_z = v_{z0} + \varepsilon v_{z1} + \varepsilon^2 v_{z2} + \ldots \quad (21)$$

$$P = P_0 + \varepsilon P_1 + \varepsilon^2 P_2 + \ldots \quad (22)$$

Substituting these into the equations and solving each order of epsilon resulted the following second order solution. (For a detailed account of the assumptions made in the derivation of these equations consult [22].)

$$v_{r1} = Re\left(r\ \text{spin}\left(-\frac{z^4}{12} + \frac{z^3}{3} - \frac{7z^2}{20} + \frac{z}{10}\right) - \frac{R_{in}}{aRer}(z^2 - z)\right) \quad (23)$$

and

$$P_0 = 0.15\ \text{spin}\ (r^2 - 1) - \left(\frac{2R_{in}}{aRe}\right)\ln(r) \quad (24)$$

The results appeared qualitatively consistent (see Figure 4) and so a higher order solution was sought. Due to the length of the polynomials, the symbolic math package 'MACSYMA' was used to carry out the algebra and the integrations. The resulting expressions are too lengthy to include herein but are listed in [22] and can be obtained from the authors. Since the velocities appear at different orders of ε (the v_r appeared at v_{r1} and v_{r3} while v_θ appeared at $v_{\theta 0}$, $v_{\theta 2}$ and $v_{\theta 4}$ and v_z at v_{z2} and v_{z4}), the calculations had to be extended to include epsilon-to-the-fourth-power terms. The unfortunate part of this was that, with increasing epsilon order, the velocity terms increased by a power of Reynolds number and/or spin, which can be, and usually are, quite large. Radial velocity comparisons between these fourth order estimates and the second order approximations, along with the numerical values generated by the FEM program, are shown in Figs 5 and 6 at two sets of parameter values.

Figures 7 and 8 report the comparisons for the other velocity components. Again a reasonable fit was obtained except for the fourth order azimuthal solution. This problem is caused by the higher order terms, including powers of Re which, in the case of the fourth order solution, apparently dominate. In the light of this, the second order approximations are more consistent over a large parameter range and will probably be the ones of choice, due to the conservative nature of the simulation that would result from their usage. Other comparisons were then done between the perturbation solution and the rigorous numerical model. Figure 9 presents the maximum axial velocity computed in the FEM model as a function of radius. After an entry length, the axial velocities approach a constant value over most of the disc until they are polluted

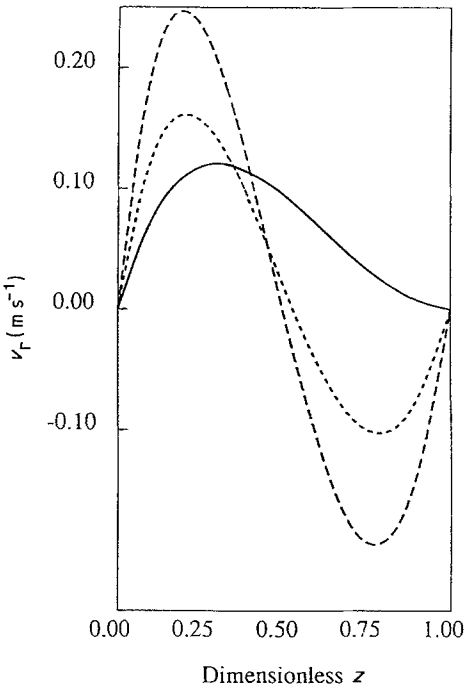

Fig. 4. Pump cell at 500 r.p.m. (α = 3.6) Semi-analytical solution: gap = 1.0 mm and flow rate = 8.33 × 10^{-7} m^3 s^{-1}. (——) r = 0.20; (– – –) r = 0.60; (— — —) r = 1.00.

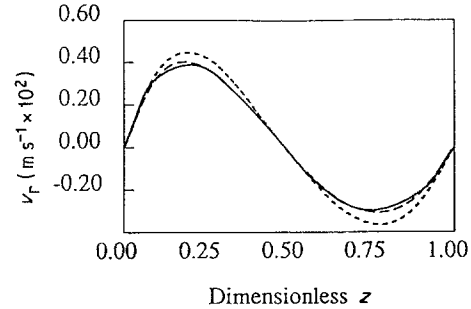

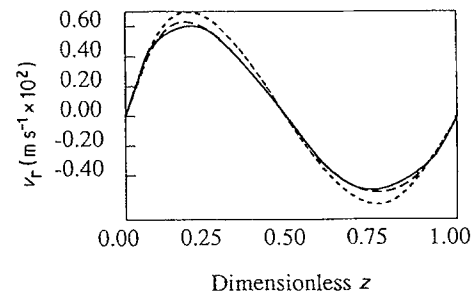

Fig. 5. Pump cell solutions at 95.5 r.p.m. (α = 1.6) Radial velocities at Re = 2, gap = 1.0 mm and flow rate = 6.28 × 10^{-9} m^3 s^{-1}. (——) FEM; (– – – –) Second order; (— — —) Fourth order.

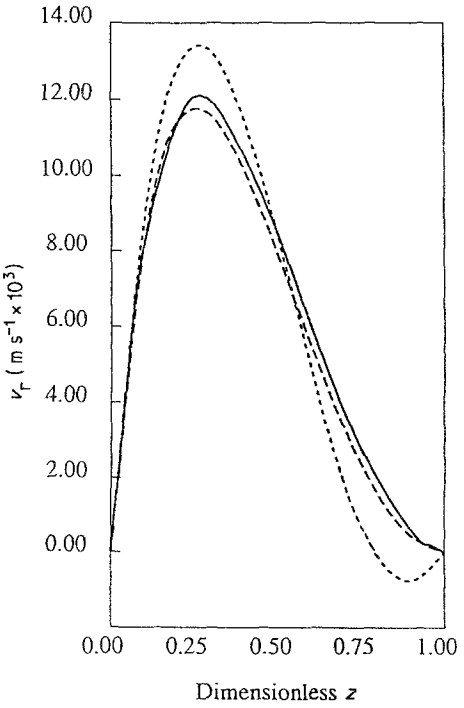

Fig. 6. Pump cell solutions at 95.5 r.p.m. (α = 1.6) Radial velocities at Re = 50, gap = 1.0 mm and flow rate = 3.14 x 10^{-7} m^3 s^{-1}. (——) FEM; (– – –) Second order; (— — —) Fourth order.

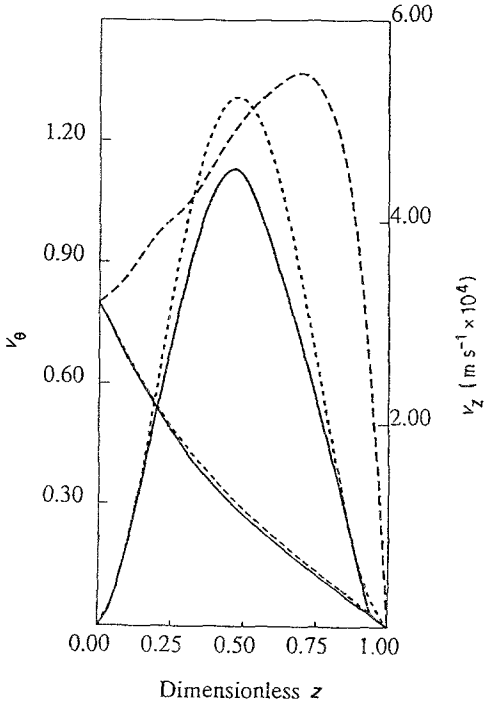

Fig. 8. Pump cell solutions at 95.5 r.p.m. (α = 1.6) Axial and azimuthal velocities at Re = 50, gap = 1.0 mm and flow rate = 3.14 x 10^{-7} m^3 s^{-1}. (——) FEM; (– – –) Second order; (— — —) Fourth order.

by the exit end boundary conditions (this influence being probably quite realistic, since the cells empty into a larger mixing tank with smaller axial velocities). This agrees well with the v_z perturbation behavior. Large gap widths were then modeled to ascertain comparative performance between the semi-analytical solution and the FEM model. Figure 10 presents the results from Fig. 2 but with the second order perturbation solution superimposed. The rotational rate is not large (only 44.4 r.p.m.), however the gap is 3.2 mm corresponding to a Taylor number of 3.4. For this parameter range the agreement is only qualitative. A modification was then included which corrects the radial and axial velocities for large Taylor numbers; the agreement is excellent for an α of 0–4.0 for both radial and axial velocities. By comparison to the GFEM results the modification is of the form: exp $(-0.14(\alpha-0.60)^2)$; for α values less than 0.60 no correction is invoked. The approach is to correct the positive radial velocity jet by the above expression and then to compute a similar factor for the negative velocity jet which will conserve mass. For the axial velocities the above exponential factor is simply applied.

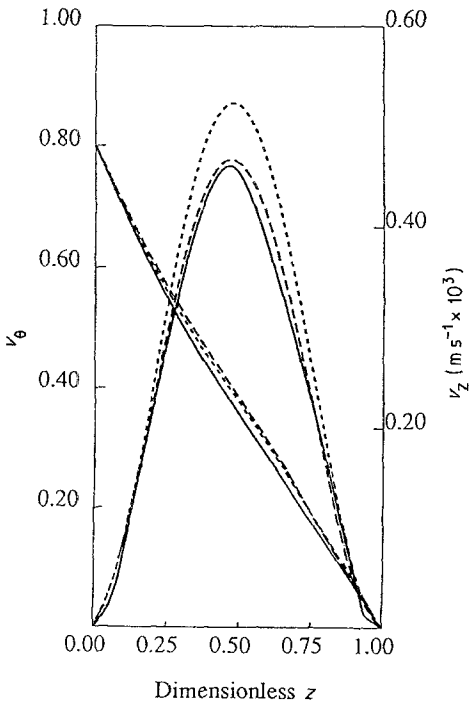

Fig. 7. Pump cell solutions at 95.5 r.p.m. (α = 1.6) Axial and azimuthal velocities at Re = 2, gap = 1.0 mm and flow rate = 6.28 x 10^{-9} m^3 s^{-1}. (——) FEM; (– – –) Second order; (— — —) Fourth order.

Figure 11 presents a comparison of the modified solution with the previous solutions for an α of 3.42. By changing the form of the correction (exp $(-0.14(\alpha-0.60)^2)$ is adequate for $\alpha < 4.0$) higher Taylor number solutions could be approximated using the basic solution derived herein.

Figure 12 presents a comparison of azimuthal velocities for the detailed and simplified models. Note that this component is essentially constant over a region of the gap ($0.25 \leqq z \leqq 0.75$). Although the agreement is not exact, this solid body rotation, commented on before as the Batchelor branch, is observed in both solutions, again indicating the rather complete representative nature of the perturbation solution, despite its simplicity. The somewhat flat v_θ profile (over $0.25 \leqq z \leqq 0.75$) is not obtained in the numerical solution until a higher r.p.m. is reached, however. In addition, another mitigating factor is that the pump

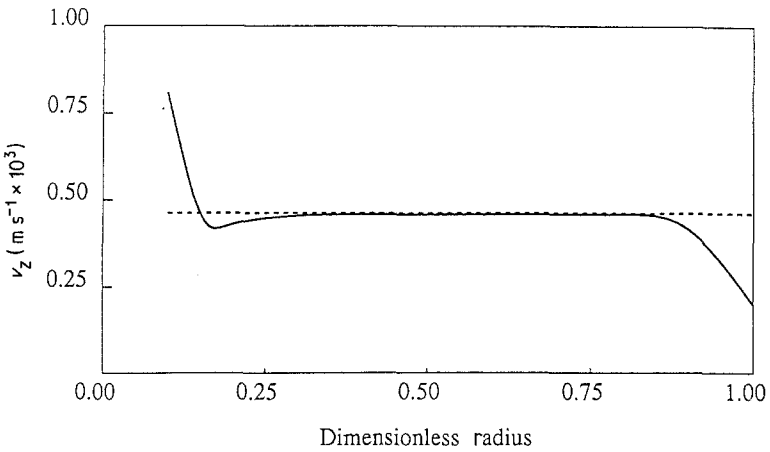

Fig. 9. Pump cell solutions at 95.5 r.p.m. Maximum axial velocities at Re = 2, gap = 1.0 mm and flow rate = 6.28 × 10^{-9} m^3 s^{-1}. (——) FEM; (- - - -) Second order.

cells are most often operated at small gap widths. Since the Taylor number is proportional to gap width but proportional to the square root of rotational speed, a decrease in gap width allows the factor squared increase in r.p.m. to maintain the same α. Therefore, if a Taylor number of 2.2 is used with a 2 mm gap width (large for pump cell applications), the cell r.p.m. would be 46.2; not very high indeed. If the gap were decreased to 1 mm (still large for the pump cell), the rotational speed could be increased to 184.9 r.p.m. If the aspect ratio is 100 (most industrial cells would be at least 100), the Re_θ would then be 1.9×10^5 which is very close to the onset of turbulence at the exit radius. Since this work is confined to laminar systems, the semi-analytical solution developed herein provides a consistent and adequate flow field representation to the pump cell over a wide parameter range. Since the solution is of a simple algebraic form, a function of radius, axial distance and dimensionless groups, it is very easy and cheap to employ. In addition, the modification included gives this semi-analytical solution a significantly broader range of application.

One interesting characteristic, which in the context of the literature review included herein has never been reported, is the radial velocity profiles at large Taylor number. Figure 13 presents a plot of v_r at a gap width of 6.4 mm, rotational speed of 45.7 r.p.m. (α = 7) and a flow rate of 229 cm^3 min^{-1} (Re = 96). Rather than exhibiting the conventional double hump shape (one positive and one negative), there is a somewhat stagnant zone in the central region of the map. Figure 14 presents the corresponding axial and azimuthal components for this system. The axial profile is much flatter than for smaller Tayler number runs; the azimuthal velocity however is much the same as before, exhibiting the somewhat flat portion over a large segment of the gap. This behavior (that of the somewhat stagnant radial velocities) agrees qualitatively with the observations of Jansson *et al.* [5]. Their observation

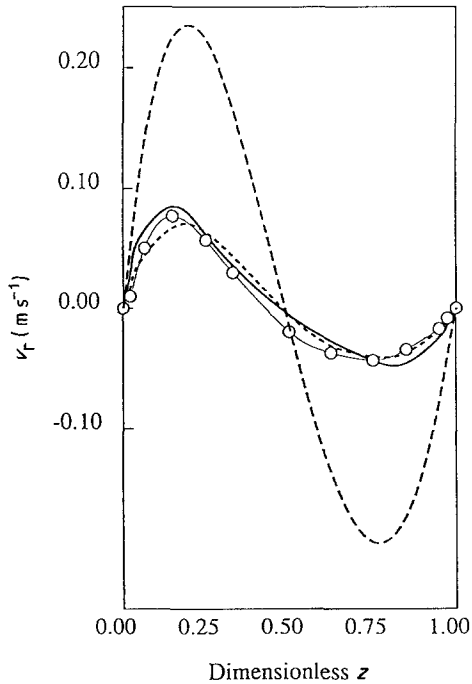

Fig. 10. Pump cell comparisons at 44.4 r.p.m. Radial velocities at R = 12.7 cm, gap = 3.18 mm and flow rate = 2.0 × 10^{-5} m^3 s^{-1}. Taylor number (α) = 3.42. (——) FEM; (- - - -) Szeri's model; (— — —) Simple model; (○) Experimental data.

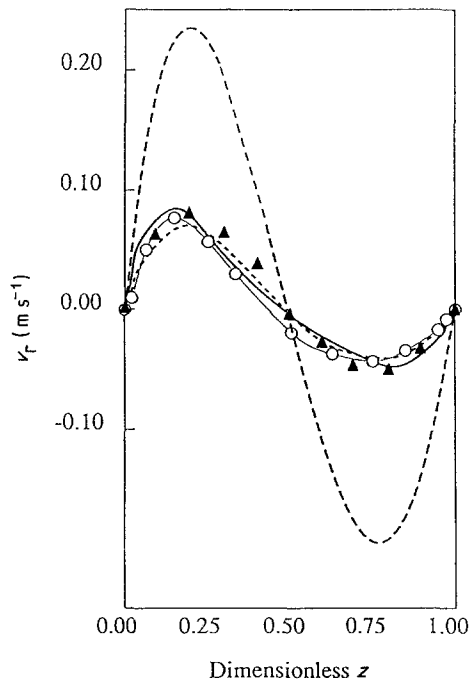

Fig. 11. Pump cell comparisons at 44.4 r.p.m. Radial velocities at R = 12.7 cm, gap = 3.18 mm and flow rate = 2.0 × 10^{-5} m^3 s^{-1}. Taylor number (α) = 3.42. (——) FEM; (- - - -) Szeri's model; (— — —) Simple model; (○) Experimental; (▲) Altered model.

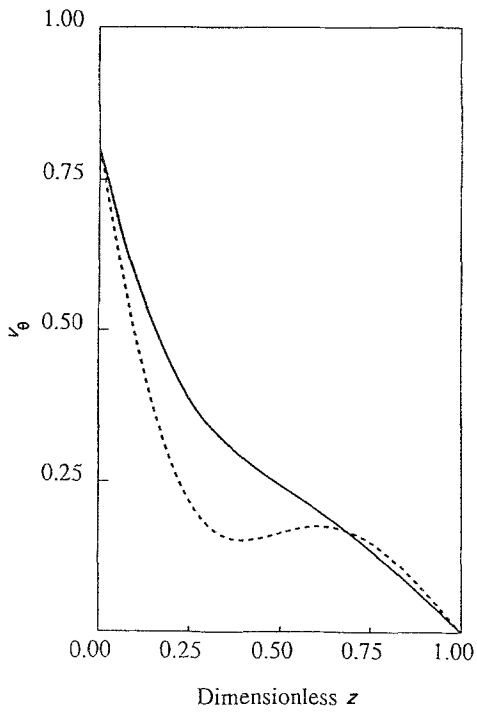

Fig. 12. Pump cell solution at 300 r.p.m. Azimuthal velocities at Re = 2, gap = 1.0 mm and flow rate = 6.28 × 10^{-9} $m^3 s^{-1}$. Taylor number (α) = 2.8. (——) FEM; (- - - -) second order.

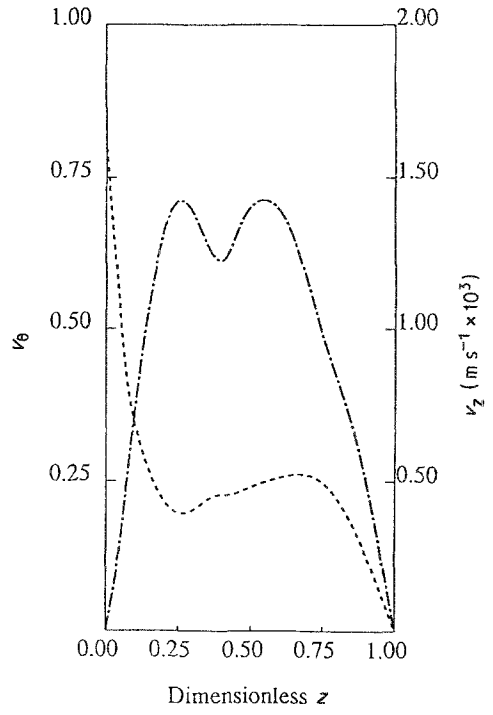

Fig. 14. Pump cell solution at 45.7 r.p.m. Axial and azimuthal velocities at Re = 96, gap = 6.4 mm and flow rate = 3.82 × 10^{-6} $m^3 s^{-1}$. Taylor number (α) = 7.0. (—·—·) Axial velocity; (- - - -) Azimuthal velocity.

(based on current density versus gap width experiments) was that current density, at a specified rotational speed, reached an asymptote on a current density–gap width plot, beyond which increasing gap resulted in no change in current. They concluded that this indicated a decoupling of the anode and cathode layers, after which the electrodes respond as if each were in a semi-infinite medium. Figure 13 substantiates this interpretation, showing that there is a boundary layer

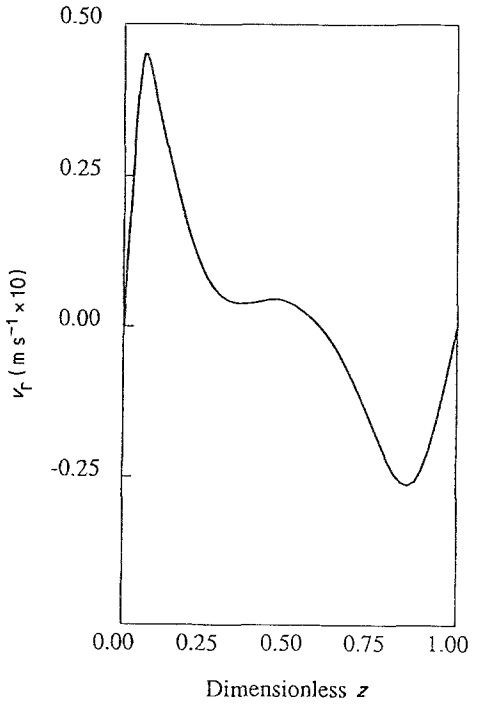

Fig. 13. Pump cell solution at 45.7 r.p.m. Radial velocities at Re = 96, gap = 6.4 mm and flow rate = 3.82 × 10^{-6} $m^3 s^{-1}$. Taylor number (α) = 7.0.

at each electrode separated by a relatively stagnant zone of fluid. There is, however, coupling still present, since the axial velocities are unidirectional. Therefore fluid leaving the reverse-flow region is carried into the bulk and then to the radial outflow region. Since the residence time of the central region is different from the radial jet close to the spinning disc (approximately an order of magnitude larger), this may impact the cell performance depending on the reaction schemes present. In addition, since the somewhat stagnant region may act as a 'reservoir' for electroactive components, one may see a reduced interplay between the electrode (anode/cathode) processes, although an actual decoupling may or may not be seen depending on the relative sizes of the three zones (anolyte, the somewhat radially stagnant bulk and the catholyte). This behavior was not predicted by the simplified solution and was not seen in any pump cell velocity simulations with Taylor numbers less than about 5.0. The observations of Jansson *et al.* [5] were at rotational Reynolds numbers well above 3 × 10^5, indicative of transition between laminar and turbulent flows, and therefore no more conclusive evidence is available concerning the role of this stagnant zone in the decoupling of mass transfer between closely spaced discs.

4.3. *Rotating electrolyzer*

This cell, briefly described as two coaxial co-rotational discs, was modeled using the same GFEM program that was employed for the other two cells. Surprisingly it exhibited many of the same characteristics as the capillary gap cell. After a certain entry length, rv_r approaches a function of z only. Figure 15 illustrates

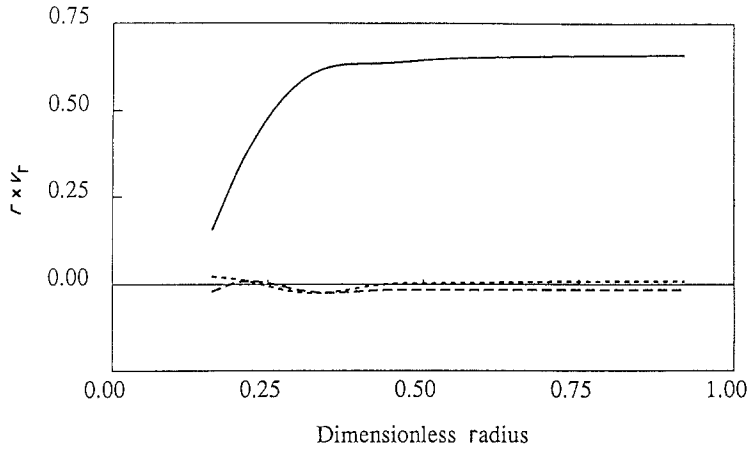

Fig. 15. Rotating electrolyzer at 120 r.p.m. Entry length information at Re = 96, gap = 6.4 mm and flow rate = 3.82 × 10^{-6} m^3 s^{-1}. Taylor number (α) = 11.3. (——) z = 0.03, 0.97; (- - - -) z = 0.25, 0.75; (— — —) z = 0.50.

this. The axial velocities were much smaller than in the pump cell, and from continuity, since rv_r is a function of z only, then

$$\frac{\partial(rv_r)}{\partial r} + \frac{\partial(rv_z)}{\partial z} = 0 \qquad (25)$$

therefore $r \times (\partial v_z/\partial z) = 0$, meaning that v_z is either a constant, or a function of radius only. Since no-slip is obeyed at the electrodes, v_z must approach zero across the gap in order for $\partial v_z/\partial z$ to be consistent. It should also be noted that Fig. 15 presents the rv_r asymptotes for the same parameter values as were used in generating Fig. 3 for the CG cell. The required entry length was considerably larger in the stationary cell than in the rotating electrolyzer. For an approximate idea of entry length, the asymptotic solution could be used (Equation 15) for the REL as well; indeed, it will provide a more accurate estimate for the REL entry length since they are always smaller than those of the CG cell; the asymptotic solution provided smaller entry regions than were actually the case for the CG cell.

Figure 16 presents a plot of the radial velocity profiles at three Taylor numbers (3.1, 7.0, 11.3). As the Taylor number increases, the radial velocity profile becomes progressively steeper. The form of the radial velocity profile, as a function of flow rate, is described in Fig. 17 for a Taylor number of 11.3. As is evident, the radial velocity profile is very insensitive to flow rate. At higher flow rates the profiles are slightly more smooth, but it is thought that this small change in shape would not be important in terms of impact on cell performance. Once the Taylor number is specified, one can utilize the same profile at any flow rate (laminar flow), taking into account the flow rate dependence of the entry region. This provides an important simplification to the rotating electrolyzer flow field. It was thought that by providing a correlation for radial velocity profiles (as a function of Taylor number and gap width) great economy could be gained. To pursue this idea the profiles were first fitted by nonlinear least squares with the coefficients to be correlated with Taylor number. This method would work well for low Taylor numbers, where the profile is somewhat smooth, but for α above about 3.5 the profiles were inadequately represented via polynomials: sixth order polynomials were required to gain an adequate fit for the radial velocity profiles (as a function of z — 7 points were used (hence, a perfect fit)), but when velocities were generated at intermediate z values, they were completely unrealistic. Other forms of expressions could be employed (other than polynomials), but it is thought that with very steep gradients, as seen in Fig. 17, no simple form may be adequate and hence no further effort was expended here. Since the simulations developed herein are based upon azimuthal symmetry, little has been mentioned of their form. Relative to that theme, the azimuthal velocities were very uniform approaching solid body rotation, especially at the lower flow rates. As flow rate increases, there is more velocity lag between the discs and the bulk of the fluid. Indeed, Jansson [3] reports negative azimuthal velocities at flow Reynolds numbers above 2100; they are particularly pronounced at smaller radii. This was not confirmed in this work due to discretization requirements and lack of computational power, although as flow rate was increased, larger lags

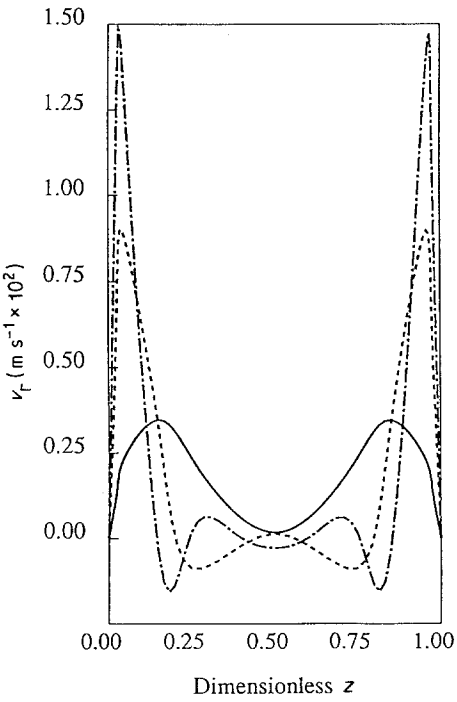

Fig. 16. Rotating electrolyzer solutions. Radial velocities with changing Taylor number: gap = 6.4 mm and flow rate = 3.82 × 10^{-6} m^3 s^{-1}. (——) α = 3.1; (- - - -) α = 7.0; (— · — · —) α = 11.3.

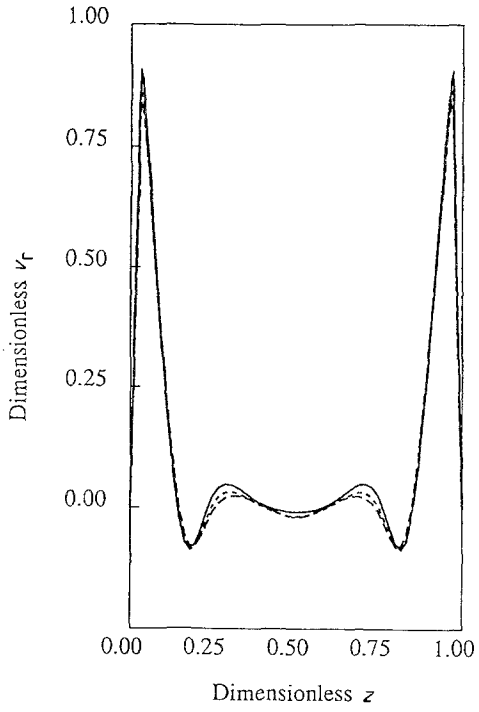

Fig. 17. Rotating electrolyzer solutions. Radial velocities with changing flow rates: gap = 6.4 mm and Taylor number = 11.3. (——) Re = 10; (– – –) Re = 288; (— – —) Re = 544.

between bulk fluid and the electrodes were observed as mentioned above.

5. Summary

The flow fields present in the three radial flow cells were simulated using finite element methods and for the case of the pump cell, a perturbation technique was developed.

The FEM program provided very good quantitative agreement with previous results (both experimental and theoretical) and proved to be more stable than some similar codes developed earlier [15].

The general forms of the velocities were confirmed and it was shown how the CG cell and REL exhibit the same radial velocity asymptotic behavior with the corresponding axial velocities approaching zero.

The pump cell was more difficult to quantify, but with the development of second and fourth order perturbation solutions, the flow field is adequately described over parameter ranges at which pump cells are usually operated (confined to laminar operation however). This semi-analytical solution provides representative velocities even for developing flow, although the vortex region, after rounding the sharp corner at the inlet pipe radius, is not accounted for.

An approximate asymptotic expression for entry length was derived for the CG cell, which is also applicable to the REL. It was found that rotation in the REL provides a stabilizing influence in terms of entry length requirements; all other conditions being the same, entry length for the REL is less than that of the CG, becoming smaller as Taylor number increases. The asymptotic expression for entry length provided a qualitative description of entry length dependence on gap width and flow rate. It, however, provided no dependence on inlet pipe radius, which was observed to have a stabilizing influence (shorter entry length) as it increased for given flow rate.

At large Reynolds numbers (above 220) two regions of separation were observed in the capillary gap simulation, one at each disc, one starting as the other one diminished. This behavior was also reported by Yang [9] in experimental studies. To explore this, a transient model will be required which would be recommended as future work.

The insensitivity of REL radial velocity profiles to flow rate was shown. In addition, the separation efficiency of the REL was described in terms of the radial velocity jets which form next to the electrodes. The larger the Taylor number the better the separation.

A high Taylor number pump cell simulation was performed which tended to substantiate, in terms of velocity profiles, the decoupling of electrodic mass transfer (anode and cathode mass transfer) as observed by Jansson [5]. At Taylor numbers beyond about 5, a relatively stagnant radial velocity region was observed. This could act as a large 'reservoir' of electroactive components, playing the role of the semi-infinite medium for each electrode.

Subsequent papers will apply the developed velocity profiles to overall simulation of the laminar radial flow cells.

Acknowledgement

The authors express their appreciation to Monsanto Corporation for their support of this project over the years 1984 to 1987. They would also like to thank Hycal Energy Research Laboratories for covering the costs of publication.

References

[1] R. E. W. Jansson and G. A. Ashworth, *J. Appl. Electrochem.* **7** (1977) 309.
[2] R. E. W. Jansson and N. R. Tomov, *Chem. Ind.* 4 Feb. (1978) 96.
[3] R. E. W. Jansson, *Electrochim. Acta* **23** (1978) 1345.
[4] G. A. Ashworth and R. E. W. Jansson, *Electrochim. Acta* **22** (1977) 1295.
[5] R. E. W. Jansson and G. A. Ashworth, *Electrochim. Acta* **22** (1977) 1301.
[6] S. Mochizuki, W. J. Yang, Y. Yagi and M. Ueno, *J. Heat Transfer* **105** (1983) 598.
[7] A. Z. Szeri, S. T. Schreider, F. Labbe and H. N. Kaufman, *J. Fluid Mech.* **134** (1983) 103.
[8] P. S. Moller, *Aeronaut. Quart.* May (1963) 163.
[9] W. J. Yang, 'Seminar on Flow between Parallel Discs with Simultaneous Heat Transfer', Washington University, St. Louis, MO, Dec. (1985).
[10] F. J. Bayley and J. M. Owen, *Aeronaut. Quart.* Nov. (1969) 333.
[11] H. Schlichting, 'Boundary Layer Theory', 7th edn, McGraw-Hill, St. Louis (1979) pp. 102–107.
[12] G. K. Batchelor, *Quart. J. Mech. Appl. Math.* (1951) 4, 29.
[13] K. Stewartson, *Proc. Camb. Phil. Soc.* **49** (1953) 333.
[14] M. Holodniok, M. Kublcek and V. Hlavacek, *J. Fluid Mech.* **81** (1977) 689.
[15] M. L. Adams and A. Z. Szeri, *J. Appl. Mech.* **49** (1982) 1.
[16] F. Kreith, *J. Heat Mass Transfer* **9** (1966) 265.
[17] R. E. W. Jansson, R. J. Marshall and J. E. Rizzo, *J. Appl. Electrochem.* **8** (1978) 281.

[18] M. Simek and I. Roušar, *Coll. Czech. Chem. Commun.* **49** (1984) 1122.
[19] P. M. Gresho, R. L. Lee and R. L. Sani, in 'Recent Advances in Numerical Methods in Fluids' (edited by C. Taylor and K. Morgan) Pineridge Press, Swansea, UK (1980) Vol. 1, pp. 27–79.
[20] B. A. Finlayson, 'Nonlinear Analysis in Chemical Engineering', McGraw-Hill, New York (1980) pp. 230–271, 291–312.
[21] P. Hood, *Int. J. Num. Meth. Engng* **10** (1976) 379.
[22] F. B. Thomas, 'Modeling of Laminar Radial Flow Electrochemical Cells', D.Sc. Thesis, Washington University, St Louis, MO August (1987).